Fabrication and evaluation of poly(lactic acid), chitosan, and tricalcium phosphate biocomposites for guided bone regeneration

Journal of Applied Polymer Science

Fabrication and evaluation of poly(lactic acid), chitosan, and tricalcium phosphate biocomposites for guided bone regeneration

Srikanthan Ramesh [1], Lisa Lungaro,[2] Dimitrios Tsikritsis,[2] Eric Weflen,[1] Iris V. Rivero [1], Alistair P. D. Elfick[2]

[1]Department of Industrial and Manufacturing Systems Engineering, Iowa State University, Ames,, Iowa 50011
[2]Institute for Bioengineering, University of Edinburgh, Mayfield Road, Edinburgh, EH9 3DW, UK
Correspondence to: I. V. Rivero (E-mail: rivero@iastate.edu)

ABSTRACT: This study presents and evaluates an approach for fabricating poly(lactic acid) (PLA)/chitosan (CS)/tricalcium phosphate (TCP) electrospun scaffolds for guided bone regeneration, a dental procedure that uses membranes to direct and delineate regions of osteogenesis. Biomaterials were pre-processed using cryomilling, a solid-state grinding technique that facilitates the generation of powdered biocomposites conducive to electrospinning. X-ray diffraction (XRD) confirmed the generation of cryomilled blends consisting of PLA, CS, and TCP. Results from the differential scanning calorimetry showed an upward shift in glass transition temperature and an increase in crystallinity with the inclusion of TCP reinforcing the observations from XRD. Murine macrophages were used to confirm the biocompatibility of the cryomilled powders and was evaluated using CellTiter-Blue (CTB) cell viability assay and brightfield microscopy. Scanning electron microscopy was used to examine the morphology of the fibers produced via electrospinning, while Raman spectroscopy confirmed material homogeneity. *In vitro* studies with MG-63 cells validated the capacity of composite scaffolds to encourage proliferation, while Coherent anti-Stokes Raman scattering and fluorescence microscopies provided visual evidence of cell proliferation. CTB assay revealed that cells maintain viability and metabolic activity at 3 and 7 days after seeding, demonstrating the potential of the biocomposite membranes. © 2018 The Authors. Journal of Applied Polymer Science published by Wiley Periodicals, Inc. J. Appl. Polym. Sci. **2018**, *135*, 46692.

KEYWORDS: biomaterials; biomedical applications; blends; composites; fibers

Received 13 January 2018; accepted 7 May 2018
DOI: 10.1002/app.46692

INTRODUCTION

In the recent years, increasing interest in developing dental procedures for bone regeneration has been driven by the growing number of patients requiring such interventions. Data from National Health and Nutrition Examination Survey (NHANES) suggests that 64.7 million adults in the USA suffer from periodontitis, a dental disease characterized by the destruction of the connective tissue and dental bone.[1] Guided bone regeneration (GBR), when applied, has been able to treat bone defects caused by periodontitis.[2] In principle, GBR uses barrier membranes to prevent the entry and proliferation of non-osteogenic cells in defect sites by selectively promoting the growth of osteogenic cells.[3] Therefore, the procedure's success, among other factors, is also largely dependent on the design and performance of the barrier membrane. A suitable barrier membrane is expected to possess biocompatibility, mechanical strength, and pliability at the time of implantation.[4] Expanded polytetrafluoroethylene (e-PTFE) has dominated as the material for the fabrication of non-resorbable membranes which needs to be surgically removal.[5] However, resorbable membranes offer an interesting alternative making the process more patient-friendly.[6] Polymers such as chitosan (CS), collagen, poly(lactic acid) (PLA), poly(ε-caprolactone) (PCL), and poly(lactic-*co*-glycolic acid) (PLGA) have been used individually, or in blends, for the fabrication for such membranes.[7]

In recent years, there has been an increased focus in the development and investigation of new polymeric blends that can possess superior mechanical and biological properties in comparison to commercially available single biopolymers. For example, Guo *et al.*[8] reported the potential of PLGA/PLLA/PDLA blend fibers loaded with naringin for GBR. In another study, a mixture of chitosan, collagen, and poly(ethylene oxide) was used to make up a nanofiber

chitosan-collagen membrane to be used in GBR.[9] Currently, the enhancement of polyester-based membranes by the addition of inorganic and organic materials is also being investigated widely.[10–12] In that regard, this study explores and evaluates the preparation approach and performance of novel biocomposite membranes consisting of PLA, CS, and tricalcium phosphate (TCP).

CS, a natural occurring biodegradable polymer, has antimicrobial properties that are desirable in resorbable membranes but inferior mechanical properties and unsuitable degradation rate have limited its exclusive use.[13,14] On the other hand, PLA, a synthetic polymer known for its suitable mechanical strength and biocompatibility has been used in the fabrication of commercially available membranes for two decades now.[15] Despite these favorable properties, the release of oligomers and acid byproducts during degradation has necessitated the need to tune its properties with ceramic fillers such as TCP.[16] Apart from being used to enhance the material strength, TCP also ensures the presence of an ideal ionic environment for bone regeneration. Composite materials thus facilitate the fabrication of tailor-made membranes that can exhibit positive synergistic effects. However, the challenges of attaining uniform dispersions and the possible denaturing of biomolecules remain a hurdle to the success of traditional compatibilization strategies.[17]

To overcome the above-mentioned challenges associated with mixing strategies, cryomilling, a solid-state, low temperature grinding process was employed in this study to generate blends of PLA, CS, and TCP. Electrospinning was then utilized to fabricate fibrous membranes due to its previous success in bone tissue engineering.[18] Material properties of cryomilled biocomposites and electrospun fibers were analyzed using X-ray diffraction (XRD), differential scanning calorimetry (DSC), scanning electron microscopy (SEM), and Raman spectroscopy. Murine macrophages (RAW 264.7) were used to investigate the cytocompatibility of the biocomposite powders via CellTiter-Blue (CTB) cell viability assay. The electrospun membranes were also evaluated for their capacity to support the growth of model osteoblasts (MG-6f3 osteosarcoma cells) using CTB cell viability assay as seen elsewhere.[19–21] A second viability assay employing fluorescence and coherent anti-Stokes Raman scattering (CARS) microscopies allowed simultaneous imaging of the fibers and cells.

In this manner, this research validates an effective approach for the fabrication of novel poly(lactide)-based biocomposites membranes through morphological, thermal, and structural characterization. In addition, this work also serves as a preliminary study for using novel PLA/CS/TCP blends for GBR applications by studying the attachment of MG-63 cells on the generated biocomposites scaffolds.

EXPERIMENTAL

Fabrication of Powder Biocomposite

PLA (Purasorb PL 10; Purac, The Netherlands), CS (448877-50G, Medium M_w; Sigma-Aldrich, Irvine, UK), and TCP (C5267-100G, 34.0–40.0% Ca basis; Sigma-Aldrich) were cryomilled to generate powdered composites. Compositions of the blends prepared in this study is as follows: A0: 100% PLA; A1: 70% PLA, 30% CS; A2: 68% PLA, 30% CS, 2% TCP; A3: 66% PLA, 30% CS, 4% TCP. The sample-containing vials were loaded into the freezer mill (6870; SPEX, Metuchen, NJ) which was maintained at −196 °C. The samples were cryomilled for 20 min (4 milling cycles).[22] A cooling time of 1 min was allowed between successive cycles and a precool time of 15 min was utilized to ensure homogeneity in temperature at the time of milling.[23] The samples were stored in a silica-filled desiccator for at least 48 h at room temperature before further processing or analysis.

Characterization of Powder Biocomposite

Confirmation for the production of a composite blend was achieved using the Rigaku Miniflex 600 XRD analysis unit (Tokyo, Japan) equipped with a Cu-Kα radiation source (λ = 0.154 nm). The voltage and current applied were 30 kV and 15 mA, respectively. The scan ranged from 3° to 80° with steps of 0.02°.

Thermal characterization of the powders produced was performed using a differential scanning calorimeter (DSC) (Phoenix, NETZSCH Instruments, Burlington, MA). To avoid the degradation of CS, the method of Sakurai *et al.*[24] was used with modifications. Suyatma *et al.*[25] reported the success of the modified method in characterizing PLA/CS biodegradable films. 8 mg of the sample were quenched at 10 °C min^{-1} to −30 °C before being heated to 190 °C at the same rate. The samples were held at 190 °C for 1 min before being cooled down to −30 °C. The samples were then held at −30 °C for 3 min before the second heating cycle in which the samples were heated to 250 °C. The second heating scan was used to identify the glass transition and melting temperatures along with percent crystallinity. Proteus Thermal Analysis version 6.1.0 was used for the analysis.

Cytotoxicity Study for Biocomposite Powder

Powders A0, A1, A2, and A3 were weighed and suspended in a standard DMEM medium (Sigma-Aldrich) at a concentration of 0.84% w/v, creating four different stock media. Each stock medium was then autoclaved at 121 °C for 15 min, cooled to room temperature, and diluted using the standard medium to give particle dose concentrations of 0.3×10^6, 1×10^6, 3×10^6, and 5×10^6 particles mL^{-1}. The dosing calculations were carried out assuming a modal particle diameter of 5 μm and a density of 1.2 g cm^{-3} for the composite material. The new solutions were named CompA0, CompA1, CompA2, and CompA3 medium.

The RAW264.7 murine macrophage cell line was used to test the cytocompatibility of CompA0-A3 medium. The cells, at passage 12, were cultivated in DMEM medium (Sigma-Aldrich) supplemented with 10% fetal bovine serum (FBS) and 1% penicillin/streptomycin (Invitrogen, Paisley, UK). When confluent, cells were trypsinized, and subsequently seeded into a 96-well plate at the concentration of 3×10^4 cells/well in a volume of 100 μL of DMEM. Cells were then incubated for 24 h at 37 °C, 5% CO_2, and subsequently exposed to CompA0-A3 media in 100 μL of medium/well. This yielded an approximate load of 10, 30, 100, and 200 particles per cell. Cells were incubated for a further 24 h and imaged using bright-field microscopy at 200× magnification (Leica Microsystem, Milton Keynes, UK). Next, CompA0-A3 media was replaced with fresh DMEM and cells were incubated for further 24 and 48 h, before proceeding with the CTB cell viability assay (Promega, Southampton, UK). Briefly, 20 μL/well of the reagent were added to cells grown in a 96-well plate which were subsequently incubated at 37 °C, 5% CO_2 for 3 h. At the end of incubation, the supernatant of each well was transferred to a fresh 96-well plate and fluorescence was measured

with a microplate reader at 560/690 nm (Modulus II Microplate Multimode Reader, Turner Biosystems, Sunnyvale, CA). Cells grown in DMEM were used as negative controls and all experiments were conducted in triplicate. Data are expressed as mean ± standard deviation (SD).

Fabrication of Resorbable Membranes

Electrospinning was employed to generate fibrous membranes using the cryomilled biocomposites. Trifluoroacetic acid (TFA) (O4902-100; Fisher Scientific) was used as the solvent. In a typical process, 18 w/v % of the cryomilled powder was added to 5 mL of TFA, and stirred using a magnetic stirrer at 25 °C for at least 24 h. A stationary copper plate covered with aluminum foil was used as the collector. The needle tip to collector distance was set to 13 cm, and the potential difference was adjusted between 15 and 17.5 kV as needed, with a flow rate of 0.05 mL min^{-1}.

Characterization of Resorbable Membranes

SEM (JCM-6000Plus NeoScope JEOL, Peabody, MA) was used to confirm the successful production of electrospun fibrous membranes. Fiber diameter was measured using JCM-6000 software version 1.1. The mean diameters of the membranes were calculated using 30 measurements from three independent samples. All diameters are represented as mean ± SD.

Further quality assurance for fiber production was conducted with NIR Raman spectroscopy. Electrospun membranes of A0, A1, A2, and A3 were cut into four different pieces and sterilized by UV irradiation for 15 min. Raman spectra were recorded at 20 different locations across each sample (4 × 5 grid with 200 μm spacing) using a Renishaw InVia microscope (785 nm excitation, 65 mW at the sample, ×40 objective giving a ~10 μm focal spot diameter). Spectra were dispersed by a 600 lines/mm grating onto a thermoelectrically cooled CCD, yielding a spectral resolution of ~7 cm^{-1} across a sampling range 400–3200 cm^{-1} wavenumbers of Stokes shift.

Performance Assessment of Resorbable Membranes

MG-63 human osteosarcoma cell line was cultivated in DMEM medium (Sigma-Aldrich) supplemented with 10% FBS and 1% penicillin/streptomycin (Invitrogen). When confluent, cells were trypsinized, and suspended into 30 μL of medium and subsequently seeded onto the scaffolds (7.5×10^4 cells/scaffold). Before cell seeding, scaffolds were placed one per well in a sterile 48-well plate, UV irradiated for 15 min and pre-soaked into DMEM for 10 min. Cell attachment was encouraged by incubating scaffolds at 37 °C, 5% CO_2 for 15 min and then 500 μL of DMEM were added to each scaffold. The media was changed every 3 days, with cell viability being investigated after 3 and 7 days using the CTB assay. At the end of the incubation period, 100 μL of CTB solution were added to scaffolds, which were incubated at 37 °C, 5% CO_2 for 3 h. Then, the supernatant from each well, together with the scaffolds, were transferred into a fresh microvial which was centrifuged at 1000 rpm for a minute. The supernatants were put into a fresh microvial and vortexed. 100 μL of the supernatants were transferred into a glass bottom microplate, and fluorescence was measured at 560/690 nm. Samples were investigated in triplicate. All data are expressed as mean ± SD.

Imaging was also used to assess cell viability using LIVE/DEAD staining (Invitrogen). The cell-laden scaffolds were incubated with Calcein acetoxymethyl (Calcein-AM) 2 μM plus ethidium homodimer-1(EthD-1) 4 μM for 15 min at 37 °C, 5% CO_2, in the dark. Scaffolds were gently washed with 1 mL of PBS post-incubation. Fluorescent dyes were excited and imaged using two-photon emission fluorescence (TPEF), while fibrous scaffolds were resolved using CARS. TPEF was read using two bandpass filters; for green fluorescence, a 515/42 nm combined with a 535/40 nm and for red fluorescent marker, the 609/54 and 640/14 nm (all Semrock). For CARS, a 1064 nm (Stokes beam) and 810.3 nm (pump beam) were used to excite the ~2940 cm^{-1} CH stretch vibration, signal was selected using a 660/13 nm bandpass filter.

Statistical Analysis

Results of the CTB cell viability assays were analyzed using PRISM version 7.0 (GraphPad Software, San Diego, CA) with 95% confidence intervals (CI) of the difference. Two-way ANOVA was performed to evaluate statistical significance with a designated Type I error rate of 0.05%.

RESULTS AND DISCUSSION

Morphology of Cryomilled Composite Powders

SEM was utilized to evaluate the morphology of the cryomilled biocomposite particles in comparison to as-received, non-cryomilled PLA. The composite powders were composed of sharp-edged particles ranging in size (across all the composite blends) from 15 to 20 μm, significantly smaller than the particle size of the materials before cryomilling [Figure 1(a,b)]. Additionally, dry agglomeration of particles was also observed.

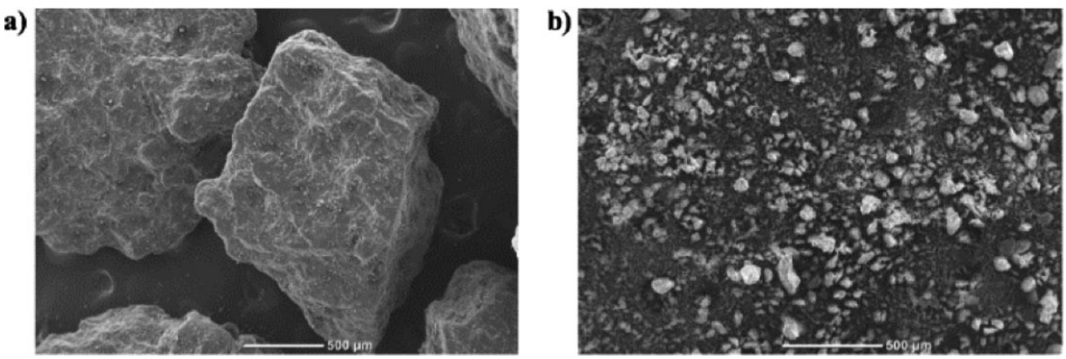

Figure 1. Representative SEM images of (a) as-received non-cryomilled PLA and (b) cryomilled PLA/CS/TCP (A3).

The primary step in the membrane fabrication process was to utilize cryomilling to generate a fine powder blend of PLA, CS, and TCP. Cryomilling, being a mechanical attrition process, subjects the materials to repeated fracturing and welding by means of collisions with a high-energy impactor bar. Other than being a solventless process, the use of cryomilling provided two benefits (a) it reduced the size disparity between the as-received PLA, CS, and TCP particles thus avoiding granular convective effects,[26] and (b) it generated a fine powder blend of dissimilar materials making it easier for dispersion in solvents. It was possible to attain a considerable reduction in particle size in short period of processing because the polymers were milled below their glass transition temperature which facilitated the occurrence of brittle fractures.[27,28] The cryomilled powders showed signs of dry agglomeration due to electrostatic and van der Waals forces between the particles.[29–31]

X-Ray Diffraction Analysis

XRD was utilized to confirm the successful production of powder blends consisting of PLA, CS, and TCP. Figure 2 shows the XRD profiles for as-received PLA, CS, and TCP along with the profiles for the composite blends prepared by cryomilling. The as-received PLA exhibited a very strong crystalline peak centered at 2θ= 16.38° and a relatively weak peak at 2θ = 18.72°. For the CS, a sharp diffraction peak was observed at 2θ = 19.44° and a weak peak centered around 2θ = 9.34°. The as-received TCP showed a lot of distinct peaks with high intensity peaks at 2θ = 25.66°, 2θ = 31.58°, and 2θ = 32.68°. All of the results for composite blends A1, A2, and A3 showed similar PLA diffraction peaks at 2θ = 16.38° and 19.44°. However, the diffractograms of all the CS-containing blends showed an increase in intensity at 2θ ≈ 20° when compared to the profile of pure PLA. For blends A2 and A3, an additional peak was observed at 2θ = 32° which appeared to grow with increasing TCP content in the polymer matrix.

PLA showed the typical profile of a semi-crystalline polymer consisting of both crystalline and amorphous regions. The positions of the peaks aligned with results reported previously.[32] The strong crystalline peak of PLA corresponded to the (110) and/or (200) plane of a typical orthorhombic crystal.[33] The two peaks shown by CS were indicative of the hydrated crystalline nature of the material.[34] The CS peaks at angles 2θ = 9.34° and 19.44° corresponded to d-spacing values of 0.95 and 0.45 nm which matched previous findings.[35] Also, TCP peaks at 2θ= 25.66°, 2θ = 31.58°, 2θ = 32.68°, 2θ = 33.86°, 2θ = 39.60°, and 46.54° confirmed the presence of TCP.[36] For all three composite blends, the increase in intensity around 2θ ≈ 20° was indicative of the presence of CS and the growing intensity of the peak around 2θ ≈ 32° with increasing TCP content reflected a successful inclusion of the ceramic component in the polymer matrix.[37] The profiles of the composite blends were observed to be influenced by those of the individual materials indicating that the materials blended only on a physical-level. On the whole, the XRD data substantiated the ability of cryomilling to generate a blend of dissimilar materials.

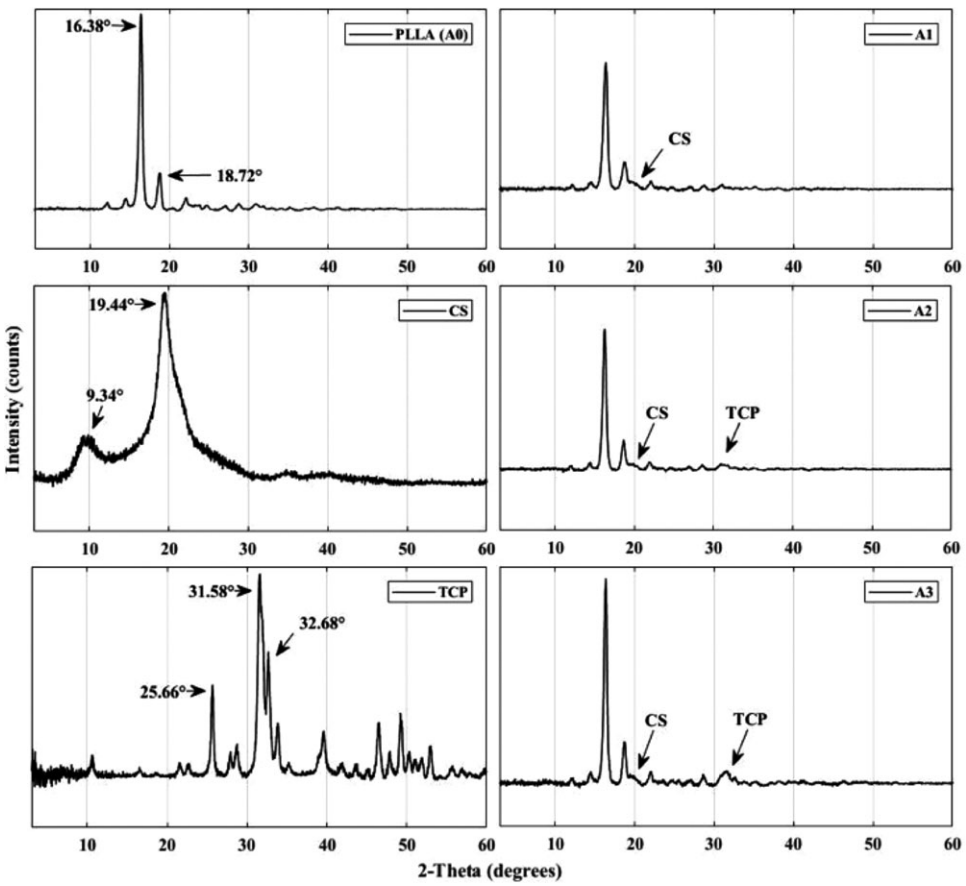

Figure 2. XRD profiles of composite blends along with their individual components.

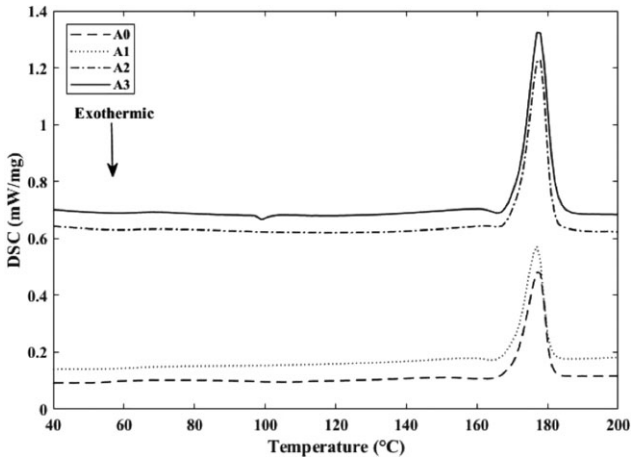

Figure 3. DSC second heating scans of the cryomilled composites.

Differential Scanning Calorimetry Analysis

DSC was used to quantify the glass transition and melting temperatures as well as crystallinity of PLA and the composite powder blends. The thermograms from the second heating scan are shown in Figure 3 while associated thermal parameters are reported in Table I. DSC curve of pure PLA revealed an average glass transition temperature of 57.6 °C followed by an endothermic melting peak at 177.5 °C with an enthalpy of fusion of 14.5 J g^{-1}. It was observed that the introduction of CS into the PLA matrix produced an increase in the glass transition temperature while decreasing crystallinity. The percent crystallinity was enhanced by the inclusion of the bioceramic, increasing to 23.9% and 27.8% with the addition of 2 and 4 wt % TCP, respectively, in comparison to the 15.2% computed for pure PLA.

The second heating scan was used to conduct the analysis as it allowed for the direct comparison of materials. The glass transition temperature of PLA obtained in this study was similar to values reported in other studies.[38] The thermogram obtained for pure PLA was indicative of its semi-crystalline nature, reinforcing the result from the diffraction study. The inclusion of CS into the PLA matrix shifted the glass transition temperature of the polymer blend (A1) upward. The semi-crystalline nature of CS, as shown in its diffraction profile, was responsible for the shift being modest. Nevertheless, the observed increase was attributed to CS obstructing the movement of PLA chains.[39] The increase in crystallinity with the addition of TCP into the polymer matrix was explained by the former acting as a nucleation agent for crystallization.[40] Since crystallinity has an influence on the rate of degradation, the degradability of scaffolds can possibly be tailored by altering the TCP content in the polymer matrix.

Morphology of Electrospun Resorbable Membranes

Figure 4 shows SEM micrographs of randomly oriented electrospun nano/microfibers of powder blends prepared in this study. As can be seen, the PLA nanofibers exhibited a round and smooth surface morphology with an average diameter of 265.83 nm. The fibers generated from PLA/CS blends displayed a similar morphology, however, with approximately a 30% increase in mean diameter with a broader distribution. The inclusion of TCP lead to the formation of significantly broader fibers of 891.83 and 1325.7 nm at 2 and 4 wt % content, respectively. The bioceramic containing fibers experienced branching and seemed to have a rougher surface even though the presence of TCP on the surface on the fibers was not evident from the micrographs.

Table I. Second Heating Scan Data from DSC Analysis

Material	T_g(°C)	T_m(°C)	X_c° (%)	H_m (J/g)
A0	57.6	177.5	15.2	14.5
A1	60.9	177	15.0	14.3
A2	62.7	177.6	23.9	22.3
A3	64	177.4	27.8	26.2

It was difficult to identify a common solvent to dissolve PLA and chitosan for electrospinning because of the inherent dissimilarity of these polymers. The benefit of using TFA was twofold (a) it facilitated the electrospinning of PLA nanofibers by increasing the solution conductivity and (b) destroyed the strong associations between chitosan molecules and thereby facilitating the continuous production of fibers.[41,42] The addition of chitosan increased the fiber diameter by enhancing the viscosity of the solution, and led to a broader distribution that was likely a consequence of increased charge density.[43] The increase of fiber diameter and distribution was reported in a previous work where similar concentrations of TCP were responsible for the inability of the polymer chains to stretch.[44] It is also likely that modifications to the viscoelastic component of the rheological behavior of the solutions changed the degree of swell experienced after extrusion from the needle. It is possible that the diameter of the fibers could have influenced cell growth.[45] Nevertheless, all the scaffolds showed promise of being structurally similar to the collagen fibers in the bone as they fell within the range 100–2000 nm and the roughness of the composite scaffolds were seen as a factor that may positively influence cell attachment.[46]

Homogeneity of Electrospun Barrier Membranes

The average Raman spectra of 20 measurements captured for the three raw materials and four electrospun composite membranes is shown in Figure 5. These measurements were carried to confirm material homogeneity after membrane fabrication.

The results of the Raman spectroscopy reinforce the findings of the powder investigation regarding the homogeneity of the material produced, and confirms this even distribution of materials is maintained in its electrospun form. As the proportion of PLA in the material falls from A0 to A3 the contribution of the PLA component of the spectrum can be seen to reduce. Additionally, it can be seen that the deviation from the mean spectrum is modest, indicating that the composition of the material was similar at all 20 sampling locations.

Cytotoxicity Study for Biocomposite Powder Blend

The cytocompatibility of the composite cryomilled powder blends was tested on a murine macrophage cell line (RAW 264.7). Results of the CTB assay [Figure 6(a,b)] indicate that 24 h after returning to cultivation in standard medium, cell viability is

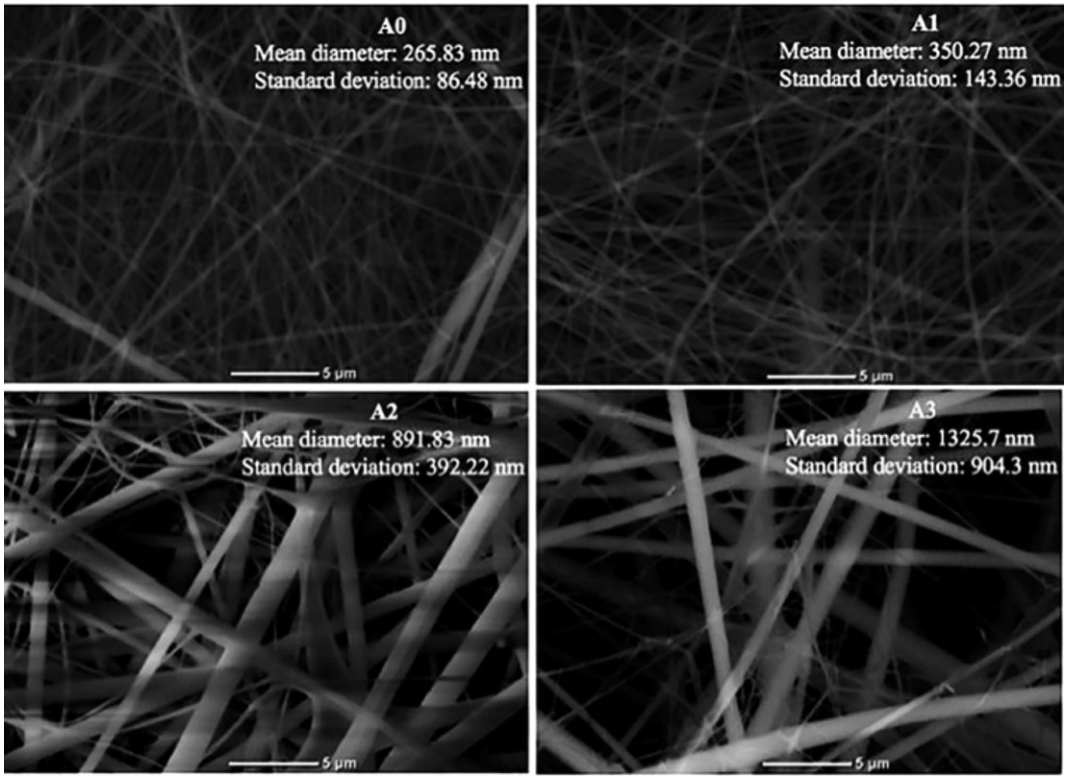

Figure 4. SEM images of fibrous membranes with fiber diameters represented as mean ± SD.

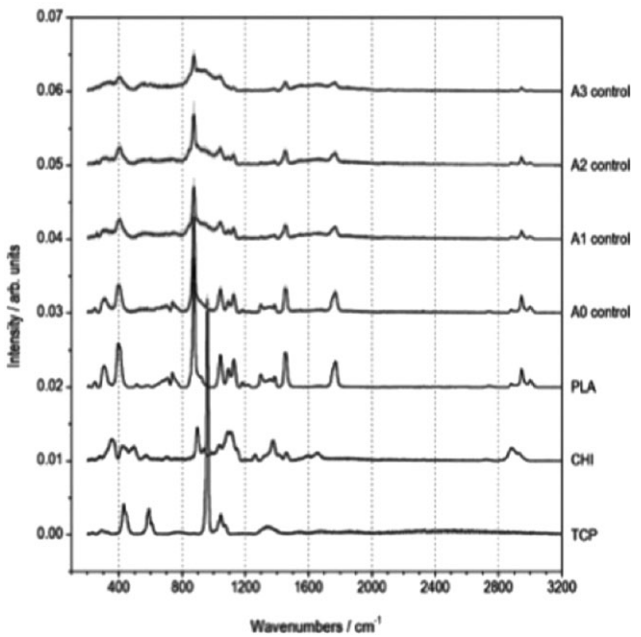

Figure 5. Baselined and normalized (to unit area) Raman spectra of each raw material (PLA, CHI, TCP) and each type of electrospun scaffold (A0, A1, A2, A3). Each spectrum represents the mean of 20 individual spectra with ±1SD.

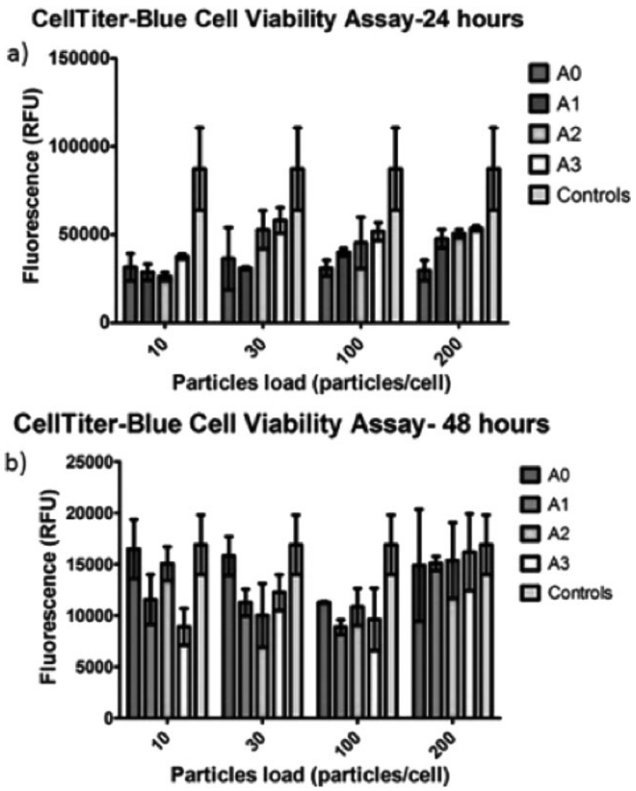

Figure 6. CTB assay performed on RAW 264.7 cell line incubated with composite cryomilled powders blend A0, A1, A2, and A3, considering different particles/cell loads, after (a) 24 h and (b) 48 h particle exposure in standard medium conditions. Results are expressed as fluorescence intensity (relative fluorescence unit-RFU) and are indicated as mean ± SD.

statistically reduced with respect to the control for all the concentrations tested. However, 48 h after returning to standard medium cultivation, the difference in cell viability between cells incubated with different cryomilled powders and controls is

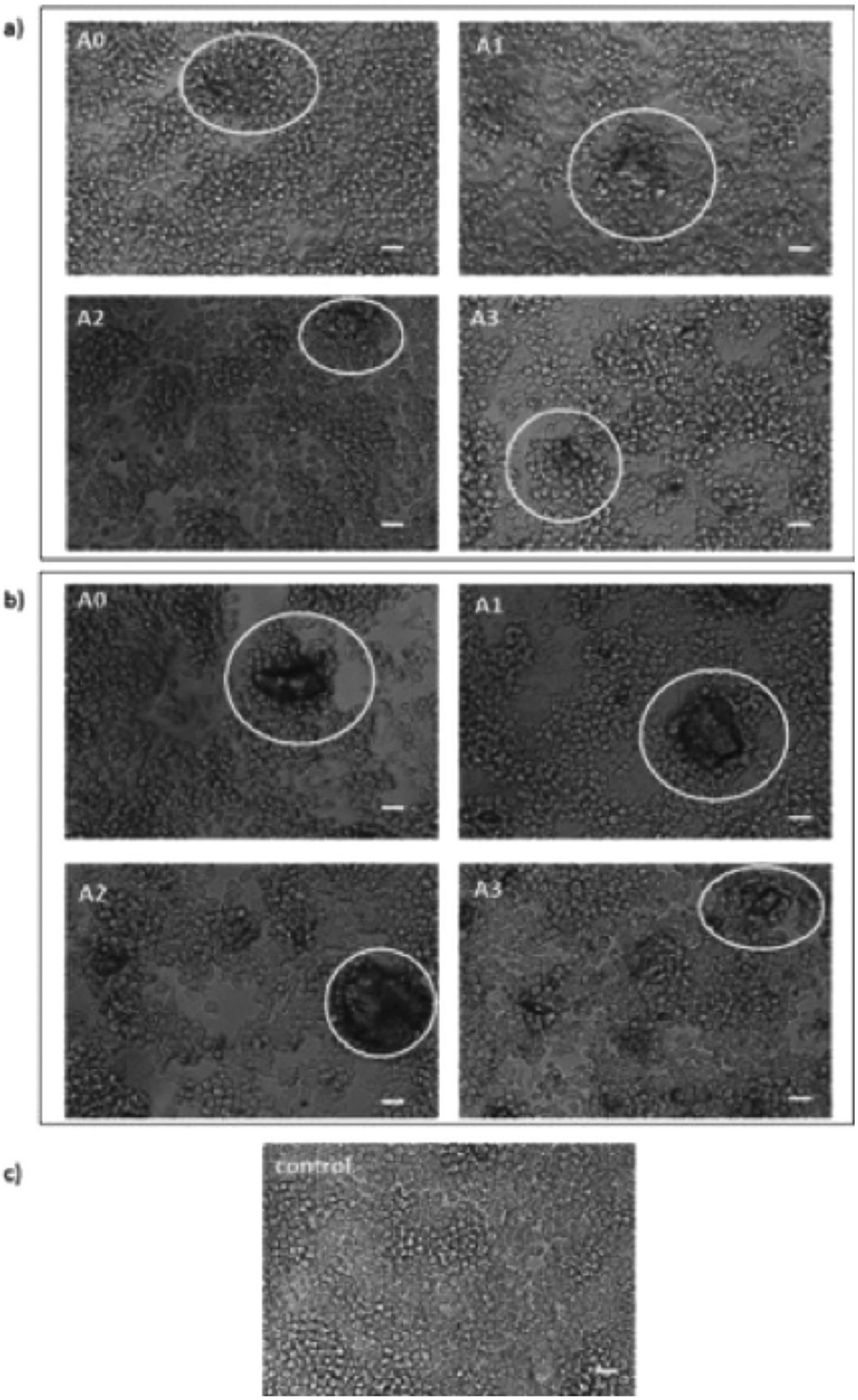

Figure 7. Representative bright-field micrographs of RAW 264.7 macrophages incubated for 24 h with different composite cryomilled powders. (a) 10 and (b) 30 particles/cell loads. (c) control; magnification = 200×; Scale bar = 20 μm.

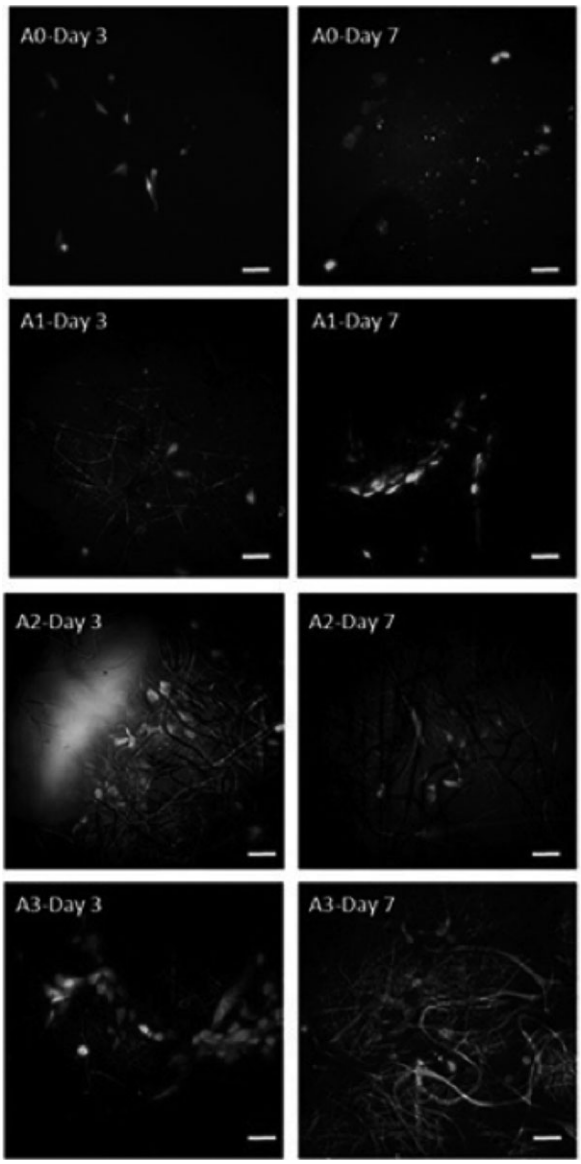

Figure 8. Fluorescence microscopy on MG-63 cells seeded into electrospun scaffolds. Scaffolds fibers are depicted using CARS; Scale bar = 20 μm.

reduced, with no statistical difference seen between controls and cells incubated with particles. Additionally, cell morphology was investigated using bright-field microscopy [Figure 7(a–c)]. No morphological changes were seen in macrophages incubated with composite cryomilled powders when compared to control macrophages grown in standard medium suggesting a low induction of phagocytic response. In addition, these micrographs reveal that particles, when suspended in culture medium, form agglomerations, to which macrophages can be seen to adhere with subsequent cell proliferation.

The high particle dose per cell in biocompatibility test represents an aggressive test of phagocytic response. The particle size formed by cryomilling lies at the upper end of the phagocytic range of macrophages.[47] Particle agglomeration, as observed *in vitro*, will act to further decrease the particles' bioavailability. The lack of morphological cues suggesting macrophagic

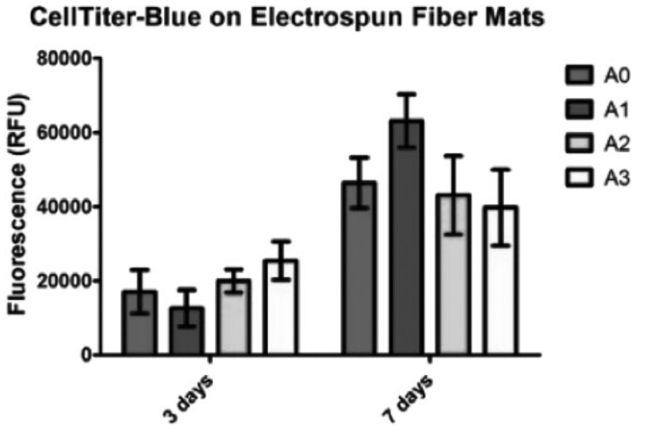

Figure 9. CTB assay performed on MG-63 cells seeded into electrospun scaffolds, after 3 and 7 days from cell seeding. Results expressed as fluorescence intensity in Relative Fluorescence Units (RFU) and are indicated as mean ± SD.

activation, and the lack of a sustained cell viability challenge (i.e., viability recovery at 48 h) indicate that the cells may not be ingesting significant numbers of particles. Importantly, neither are the cells significantly perturbed by their extracellular interaction with the biocomposite powders after an initial retardation of their proliferation. Our results suggest that particle release should not be a significant source of biocompatibility challenges.

Performance Assessment of PLA/CS/TCP Biocomposite Membranes

The viability of MG-63 cells was qualitatively examined by fluorescence and CARS microscopy at day 3 and 7 after cell seeding onto scaffolds. All the scaffolds show high cell viability and low number of dead cells, as shown in Figure 8. MG-63 cell viability was evaluated also by CTB assay, at day 3 and 7 from cell seeding into scaffolds (Figure 9). The results confirm the observations from the fluorescence investigation, showing that cells are viable at both time points investigated.

Cells were able to colonize the scaffolds, and proliferate on them. There was evidence that the scaffolds containing CS (A1, A2, and A3) appeared more suitable for cell attaching than scaffold A0, as indicated by the pictures from fluorescence and CARS microscopy, which show a higher number of cells. Scaffolds A1 and A3, in particular, were noticed to have a good cell attachment along scaffold fibers. The results of the CTB assay reflected the observations made from the qualitative analysis. There was an increase of registered fluorescence intensity, corresponding to an increase of cell viability, at day 7 with respect to day 3, indicating that cells may be able to integrate inside the scaffolds and to grow on them with the passing of days.

The aim of this study was to determine if osteoblast-like cells are able to attach and proliferate on electrospun scaffolds. Although no statistical difference was noticed among the different type of scaffolds investigated, the promising results obtained on scaffolds A1–A3 encourage additional investigations. Further study will investigate induction and maintenance of osteoblastic phenotype by following appropriate osteoblastic markers over extended periods; such as, the alkaline phosphatase activity, the formation

of calcium phosphate and the expression of osteogenic genes such as osteopontin and osteocalcin.[48]

CONCLUSIONS

Cytotoxicity testing on precursor powders used to manufacture the scaffolds reveals a response from macrophages 24 h after exposure to the powders, with their viability reduced when compared to untreated controls. Biocompatibility of micron-sized particles of material is known to diverge from the same material in the bulk; all the materials that have been utilized have established biocompatibility. While the particles lie at the upper bound of the phagocytosable range, it is likely that at the high particle loads used there will be sufficient bio-available material to impinge on cell viability. This effect could persist despite the tendency of the powders to form large agglomerates when in suspension. When nanoparticles aggregate, cytotoxicity may potentially arise from many factors, hence it is difficult to define the causal factors of macrophage activation and the ultimate cytotoxicity of the particles. However, after 48 h recovery period of cultivation in standard medium the viability of the macrophages that were challenged with particles are comparable to that of controls. This could be interpreted as a transient cell inhibition by particles, allowing the cells to restore their viability and proliferation activity. Importantly, electrospun fibers scaffolds formed by these powders show good biocompatibility and appear suitable scaffolds for osteoblast-like cells, promoting adhesion and proliferation. MG-63 cell morphology, being stellate not spherical, shows good attachment to individual fibers of the scaffolds, with the cells' growth increasing over time. These preliminary material quality and biocompatibility experiments justify further investigation into the mechanical performance of the membranes and longer-term cell response, to include osteogenesis and biodegradation studies.

REFERENCES

1. Eke, P. I.; Dye, B. A.; Wei, L.; Thornton-Evans, G. O.; Genco, R. J. *J. Dent. Res.* **2012**, *91*, 914.
2. Lee, J. Y.; Lee, J.; Kim, Y. K. *J. Dent. Sci.* **2013**, *8*, 281.
3. Retzepi, M.; Donos, N. *Clin. Oral Implants Res.* **2010**, *21*, 567.
4. Scantlebury, T. V. *J. Periodontol.* **1993**, *64*, 1129.
5. Aaboe, M.; Pinholt, E. M.; Hjorting-Hansen, E. *Br. J. Oral Maxillofac. Surg.* **1995**, *33*, 312.
6. Jung, R. E.; Fenner, N.; Hämmerle, C. H. F.; Zitzmann, N. U. *Clin. Oral Implants Res.* **2013**, *24*, 1065.
7. Wang, J.; Wang, L.; Zhou, Z.; Lai, H.; Xu, P.; Liao, L.; Wei, J. *Polymers* **2016**, *8*, 115.
8. Guo, Z.; Wu, S.; Li, H.; Li, Q.; Wu, G.; Zhou, C. *Dent. Mater.* **2018**, *37*, 317.
9. Gao, B.; Li, X. J.; Lin, M.; Li, Y. Y.; Dong, Y. *Chin. J. Stomatol.* **2018**, *53*, 85.
10. Castro, A. G. B.; Diba, M.; Kersten, M.; Jansen, J. A.; van den Beucken, J. J. J. P.; Yang, F. *Mater. Sci. Eng. C* **2018**, *85*, 154.
11. Fu, L.; Wang, Z.; Dong, S.; Cai, Y.; Ni, Y.; Zhang, T.; Wang, L.; Zhou, Y. *Materials (Basel)* **2017**, *10*, 257.
12. Arunjaroensuk, S.; Panmekiate, S.; Pimkhaokham, A. *Int. J. Oral Maxillofac. Implants* **2018**, *33*, 206.
13. Kuo, S. M.; Chang, S. J.; Chen, T. W.; Kuan, T. C. *J. Biomed. Mater. Res. Part A* **2006**, *76*, 408.
14. Bavariya, A. J.; Norowski, A. P.; Anderson, M. K.; Pradeep, A. C.; Garcia-Godoy, F.; Stein, S. H.; Bumgardner, J. D. *J. Biomed. Mater. Res. Part B: Appl. Biomater.* **2014**, *102*, 1084.
15. Galgut, P.; Pitrola, R.; Waite, I.; Doyle, C.; Smith, R. *J. Clin. Periodontol.* **1991**, *18*, 581.
16. Cao, L.; Duan, P. G.; Wang, H. R.; Li, X. L.; Yuan, F. L.; Fan, Z. Y.; Li, S. M.; Dong, J. *Int. J. Nanomed.* **2012**, *7*, 5881.
17. Allaf, R. M.; Rivero, I. V. *J. Mater. Sci. Mater. Med.* **2011**, *22*, 1843.
18. Ramachandran, K.; Gouma, P. I. *Recent Pat. Nanotechnol.* **2008**, *2*, 1.
19. Yoo, C. K.; Jeon, J. Y.; Kim, Y. J.; Kim, S. G.; Hwang, K. G. *Maxillofac. Plast. Reconstr. Surg.* **2016**, *38*, 17.
20. Kim, M. J.; Choi, H. J.; Cho, J.; Lee, J. B.; Sung, H. J.; Kim, J. K. *Int. J. Polym. Sci.* **2017**, *2017*, 1. DO: 10.1155/2017/1286109.
21. Sui, G.; Yang, X.; Mei, F.; Hu, X.; Chen, G.; Deng, X.; Ryu, S. *J. Biomed. Mater. Res. Part A* **2007**, *82*, 445.
22. Lim, J.; Chong, M. S. K.; Chan, J. K. Y.; Teoh, S. H. *Small* **2014**, *10*, 2495.
23. Jonnalagadda, J. B.; Rivero, I. V.; Warzywoda, J. *J. Biomater. Appl.* **2015**, *30*, 472.
24. Sakurai, K.; Maegawa, T.; Takahashi, T. *Polymer (Guildf.)* **2000**, *41*, 7051.
25. Suyatma, N. E.; Copinet, A.; Tighzer, L.; Coma, V. *J. Polym. Environ.* **2004**, *12*, 1.
26. György, M.; György, B.; Péter, A.; Istvan, R. *J. Polym. Eng.* **1993**, *12*, 33.
27. Zhu, Y. G.; Li, Z. Q.; Zhang, D.; Tanimoto, T. *J. Polym. Sci. Part B: Polym. Phys.* **2006**, *44*, 1161.
28. Smith, A. P.; Harald, A.; Koch, C. C.; Smith, S. D.; Spontak, R. J. *Macromolecules* **2000**, *33*, 1163.
29. Ye, J.; Han, B. Q.; Schoenung, J. M. *Philos. Mag. Lett.* **2006**, *86*, 721.
30. Zhu, Y. G.; Li, Z. Q.; Zhang, D.; Tanimoto, T. *J. Appl. Polym. Sci.* **2006**, *99*, 501.
31. Jiang, J.; Oberdörster, G.; Biswas, P. *J. Nanopart. Res.* **2009**, *11*, 77.
32. Naga, N.; Yoshida, Y.; Noguchi, K.; Murase, S. *Open J. Polym. Chem.* **2013**, *3*, 29.
33. Wu, T. M.; Wu, C. Y. *Polym. Degrad. Stab.* **2006**, *91*, 2198.
34. Wang, S. F.; Shen, L.; Zhang, W. D.; Tong, Y. J. *Biomacromolecules* **2005**, *6*, 3067.
35. Muzzarelli, C.; Francescangeli, O.; Tosi, G.; Muzzarelli, R. A. A. *Carbohydr. Polym.* **2004**, *56*, 137.
36. Siddiqui, N.; Pramanik, K. *J. Appl. Polym. Sci.* **2014**, *131*, DOI 10.1002/app.41025. doi:10.1002/app.41025
37. Spiridon, I.; Paduraru, O. M.; Zaltariov, M. F.; Darie, R. N. *Ind. Eng. Chem. Res.* **2013**, *52*, 9822.

38. Correlo, V. M.; Boesel, L. F.; Bhattacharya, M.; Mano, J. F.; Neves, N. M.; Reis, R. L. *Mater. Sci. Eng. A* **2005**, *403*, 57.
39. Tanase, C. E.; Spiridon, I. *Mater. Sci. Eng. C* **2014**, *40*, 242.
40. Mathieu, L. M.; Bourban, P. E.; Månson, J. A. E. *Compos. Sci. Technol.* **2006**, *66*, 1606.
41. Hadjizadeh, A.; Savoji, H.; Ajji, A. *Biomed Res. Int.* **2016**, *2016*, 1. DOI 10.1155/2016/8921316.
42. Lee, K. Y.; Jeong, L.; Kang, Y. O.; Lee, S. J.; Park, W. H. *Adv. Drug Deliv. Rev.* **2009**, *61*, 1020.
43. Meng, Z. X.; Zheng, W.; Li, L.; Zheng, Y. F. *Mater. Chem. Phys.* **2011**, *125*, 606.
44. Siqueira, L.; Passador, F. R.; Costa, M. M.; Lobo, A. O.; Sousa, E. *Mater. Sci. Eng. C* **2015**, *52*, 135.
45. Sisson, K.; Zhang, C.; Farach-Carson, M. C.; Chase, D. B.; Rabolt, J. F. *J. Biomed. Mater. Res. Part A* **2010**, *94*, 1312.
46. Murugan, R.; Ramakrishna, S. *Compos. Sci. Technol.* **2005**, *65*, 2385.
47. Elfick, A. P. D.; Green, S. M.; McCaskie, A. W.; Birch, M. A. *J. Biomed. Mater. Res. Part B: Appl. Biomater.* **2004**, *71*, 244.
48. Tsai, S. W.; Liou, H. M.; Lin, C. J.; Kuo, K. L.; Hung, Y. S.; Weng, R. C.; Hsu, F. Y. *PLoS One* **2012**, *7*, e31200. DOI 10.1371/journal.pone.0031200.